Three energy scales in the superconducting state of hole-doped cuprates detected by electronic Raman scattering

S. Benhabib,[1] Y. Gallais,[1] M. Cazayous,[1] M.-A. Méasson,[1] R. D. Zhong,[2] J. Schneeloch,[2] A. Forget,[3]
G. D. Gu,[2] D. Colson,[3] and A. Sacuto[1,*]

[1]*Laboratoire Matériaux et Phénomènes Quantiques (UMR 7162 CNRS), Université Paris Diderot-Paris 7,
Bâtiment Condorcet, 75205 Paris Cedex 13, France*
[2]*Condensed Matter Physics and Materials Science Department, Brookhaven National Laboratory (BNL), Upton, New York 11973, USA*
[3]*Service de Physique de l'Etat Condensé, CEA-Saclay, 91191 Gif-sur-Yvette, France*

We explore by electronic Raman scattering the superconducting state of the $Bi_2Sr_2CaCu_2O_{8+\delta}$ (Bi-2212) crystal by performing a fine-tuned doping study. We find three distinct energy scales in A_{1g}, B_{1g}, and B_{2g} symmetries which show three distinct doping dependencies. Above $p = 0.22$, the three energies merge; below $p = 0.12$, the A_{1g} scale is no longer detectable, while the B_{1g} and B_{2g} scales become constant in energy. In between, the A_{1g} and B_{1g} scales increase monotonically with underdoping, while the B_{2g} one exhibits a maximum at $p = 0.16$. The three superconducting energy scales appear to be a universal feature of hole-doped cuprates. We propose that the nontrivial doping dependencies of the three scales originate from the Fermi-surface changes and reveal competing orders inside the superconducting dome.

I. INTRODUCTION

Conventional superconductors are characterized by a single energy scale, i.e., the superconducting gap, which is proportional to the critical temperature T_c [1]. The existence of more than one energy scale in the superconducting state of hole-doped cuprates has stirred much debate for several years [2–9] and has raised the question of the existence of more than one gap in the superconducting state of cuprates [10–14]. To move toward an understanding of high-temperature superconductivity, one of the most challenging issues is the identification of the energy scales associated with the onset of coherent excitations in the superconducting state. The electronic Raman spectroscopy is an efficient probe for this task. Depending on the symmetries (A_{1g}, B_{1g}, or B_{2g}) related to the quasi-tetragonal structure of the cuprates, the energy scales can be explored in different regions of the Brillouin zone by electronic Raman scattering. Usually, the B_{1g} and B_{2g} energy scales are, respectively, assigned to the maximum amplitude of the d−wave 2Δ pairing gap in the region near $(\pm\pi,0)$ and $(0,\pm\pi)$ (called the antinodal region) and the weaker amplitude in the region near $(\pm\pi/2, \pm\pi/2)$ (called the nodal region) [15,16]. *A priori*, these two scales have the same origin (the 2Δ pairing gap) and have to follow each other. In fact, they exhibit distinct doping dependencies and are responsible for the two-gap issue in the superconducting state of hole-doped cuprates. Several distinct scenarios are still debated [5–7,10–12,16–22]. One of them has been to associate the nodal energy scale to the superconducting state, while the antinodal one is associated with the pseudogap [23,24]. Although the origin and significance of these two scales are not yet explained, a common thread is emerging: at least two electronic orders compete inside the superconducting dome of hole-doped cuprates and make distinct the doping evolutions of the B_{1g} and B_{2g} energy scales.

Competing orders are the necessary ingredients to induce Fermi-surface changes [25,26]. In hole-doped cuprates, angle-resolved photoemission spectroscopy (ARPES) revealed above T_c a disconnected Fermi surface with "Fermi arcs" centered around the nodes in an underdoped Bi-2212 compound [27]. More recently, quantum oscillation measurements under high magnetic field and low temperature have shown that the Fermi surface undergoes a reconstruction into pockets in the underdoped $YBa_2Cu_3O_{7-\delta}$ (Y-123) compound [28–31].

On the other hand, there exists a third energy scale detected in A_{1g} symmetry whose origin is still mysterious, although it has been detected for a long time [32–36]. In the Y-123 compound, the A_{1g} energy peak was found to follow the inelastic neutron-scattering resonance [37–39] with nickel and zinc substitutions [40,41]. In the very beginning of the cuprates Raman studies, the A_{1g} peak was assigned to the 2Δ pairing gap, but later considerations showed that long-range Coulomb screening washes out the gap effects in the A_{1g} geometry [15,42] and recent investigations instead advocate in favor of a collective mode [15,43,44]. However, no thorough doping evolution of the A_{1g} energy scale has been established.

In this study, our purpose is to accurately determine the actual doping dependencies of these three energy scales on a large range of doping p to get a better understanding of their origins. In particular, we are interested in finding the specific range of doping levels for which the energy scales present drastic changes and how they can be connected to the doping evolution of the Fermi surface and competing orders mentioned above.

In order to reach this goal, we have performed light polarized electronic Raman scattering on Bi-2212 single crystals, which can be associated to the $I/4mmm-D_{4h}^{17}$ space group [45]. We have the Raman spectra in A_{1g}, B_{1g}, and B_{2g} symmetries. In particular, special care has been devoted to extract the pure A_{1g} spectrum from well-controlled subtractions of the Raman spectra. Importantly, the doping level was solely controlled by oxygen insertion to avoid cationic substitutions, which can drastically change the electronic

---

*Corresponding author: alain.sacuto@univ-paris-diderot-fr

Raman spectra [46]. The large range of doping levels from $p = 0.06$ to $p = 0.23$ was successfully obtained from specific annealing treatments described in the experimental procedure. This allows us to follow simultaneously in a unique system the doping evolution of the A_{1g}, B_{1g}, and B_{2g} energy scales and even track them from very low to high doping levels.

We show that the A_{1g}, B_{1g}, and B_{2g} energy scales in Bi-2212 merge together above $p = 0.22$ and decrease with doping. This corresponds to a huge enhancement of the antinodal Bogoliubov quasiparticle spectral weight related to a Lifshitz transition where the holelike Fermi surface transforms into an electronlike one. On the other hand, the difference between the B_{1g} and B_{2g} energy scales is abnormally large below $p = 0.12$ and the B_{1g} and B_{2g} scales are almost constant with doping. This corresponds to a significant loss of the antinodal Bogoliubov quasiparticle spectral weight where charge ordering settled. Between these two doping levels, the A_{1g} and B_{1g} scales increase monotonically, while the B_{2g} scale is nonmonotonic and is peaked at $p = 0.16$ for which T_c is maximum.

II. DETAILS OF THE EXPERIMENTAL PROCEDURE

A. Raman experimental setup

Electronic Raman experiments have been carried out using a triple grating spectrometer (JY-T64000) equipped with a liquid-nitrogen-cooled CCD detector. Raman spectra above and below T_c were obtained using a closed-cycle He cryostat (Advanced Research Systems, Inc.). The laser excitation line used was the 532 nm of a diode pump solid-state laser. The laser power at the entrance of the cryostat was maintained below 2 mW to avoid overheating of the crystal estimated to 3 K/mW at 10 K. The $B_{1g}+A_{2g}$ and $B_{2g}+A_{2g}$ symmetries have been obtained from cross linear polarizations at 45° from the Cu-O bond directions and along them, respectively [47]. The change between both of these symmetries was obtained by keeping fixed the orientations of the analyzer and the polarizer and by rotating the crystal with a piezodriven rotator (Attocube). We obtained an accuracy on the crystallographic axes' orientation with respect to the polarizers close to 2°. The $A_{1g}+B_{2g}$ and $A_{1g}+B_{1g}$ symmetries were obtained from linear parallel polarizations at 45° from the Cu-O bond directions and along them, respectively. In practice, we measure the $B_{1g}+A_{2g}$ and $A_{1g}+B_{2g}$ responses and then rotate the crystal to get the $B_{2g}+A_{2g}$ and $A_{1g}+B_{1g}$ ones. In the following, we have made the assumption that the A_{2g} electronic Raman scattering contribution is negligible, i.e., the Raman vertices $\gamma_{xy} - \gamma_{yx} \approx 0$. This is supported by the very weak Raman contribution at low energy (below $1000\,\mathrm{cm}^{-1}$) in pure A_{2g} extracted from a combination of linear and circular polarization spectra [48].

All of the spectra have been corrected for the Bose factor and the instrumental spectral response. They are thus proportional to the imaginary part of the Raman response function $\chi_\nu''(\omega, T)$, where ν refers to the vertex symmetry A_{1g}, B_{1g}, or B_{2g}.

B. Crystal growth and characterization

The Bi-2212 single crystals were grown by using a floating-zone method. The optimal doped sample with $T_c = 90$ K was grown at a velocity of 0.2 mm per hour in air [49].

In order to get overdoped samples down to $T_c = 65$ K, the as-grown single crystal was put into a high-oxygen-pressured cell between 1000 and 2000 bars and then was annealed from 350 °C to 500 °C for three days [50]. The overdoped samples below $T_c = 60$ K were obtained from as-grown Bi-2212 single crystals put into a pressure cell (Autoclave France) with 100 bars oxygen pressure and annealed from 9 to 12 days at 350 °C. Then the samples were rapidly cooled down to room temperature by maintaining a pressure of 100 bars. In order to get the underdoped sample down to $T_c = 50$ K, the optimal doping crystal was annealed between 350 °C and 550 °C during three days under vacuum of $1.3 10^{-6}$ mbar. The critical temperature T_c for each crystal has been determined from magnetization susceptibility measurements at a 10 Gauss field parallel to the c axis of the crystal. More than 30 crystals have been measured among 60 tested. The selected crystals exhibit a quality factor of $T_c/\Delta T_c$ larger than 7. ΔT_c is the full width of the T_c transition measured. A complementary estimate of T_c was achieved from electronic Raman scattering measurements by defining the temperature from which the B_{1g} superconducting pair breaking peak collapses. The level of doping p was defined from T_c using Presland and Tallon's equation [51]: $1 - T_c/T_c^{\max} = 82.6(p - 0.16)^2$. T_c versus p is reported in Fig. 3(a).

III. EXPERIMENTAL RESULTS

Figures 1(a)–1(d) display the Raman responses of an overdoped (OD) Bi-2212 single crystal with $T_c = 60$ K. The red (gray) and black curves were measured below and above T_c in the $A_{1g}+B_{1g}$, $A_{1g}+B_{2g}$, B_{1g}, and B_{2g} symmetries. The sharp peaks located at 127, 297, 327, 359, and $474\,\mathrm{cm}^{-1}$ are phonon lines that will be discussed in a future paper. A comparison between Figs. 1(c) and 1(d) shows that the B_{1g} electronic contribution is preponderant compared to the B_{2g} one. It manifests itself as an intensive 2Δ pair breaking whose maximum is peaked at $244\,\mathrm{cm}^{-1}$ [see inset of Fig. 1(c)]. The B_{2g} electronic peak, although much lower in intensity, is centered around the same energy ($\approx 254\,\mathrm{cm}^{-1}$) [see inset of Fig. 1(d)].

In $A_{1g}+B_{1g}$ symmetry [Fig. 1(a)], the B_{1g} electronic contribution is dominant such that the A_{1g} electronic peak can only be observed in the $A_{1g}+B_{2g}$ response [Fig. 1(b)] since the B_{2g} contribution is weak. The A_{1g} electronic continuum [detectable in Fig. 1(b)] is maximum around $250\,\mathrm{cm}^{-1}$ nearby the energies of the B_{1g} and B_{2g} peaks.

The Raman responses in Figs. 1(e)–1(h) and Figs. 1(i)–1(l) correspond, respectively, to the optimally doped (OP) crystal ($T_c = 90$ K), $p = 0.16$, and the underdoped (UD) crystal ($T_c = 70$ K), $p = 0.11$. Examining the B_{1g} and B_{2g} Raman responses of the OP90 crystal [Figs. 1(g) and 1(h)], we can notice that the B_{1g} electronic contribution remains predominant compared to the B_{2g} one, although the B_{1g} Raman response is significantly reduced in intensity with respect to the OD60 compound. The energies of the B_{1g} and B_{2g} superconducting peaks [see insets of Figs. 1(g) and 1(h)] are still close to each other. Interestingly, the energy of the A_{1g} peak is observable in $A_{1g}+B_{2g}$ symmetry [Fig. 1(f)] and its energy is clearly distinct ($\approx 350\,\mathrm{cm}^{-1}$) from those of B_{1g} and B_{2g} peaks located instead around $500\,\mathrm{cm}^{-1}$. Concerning the UD70 Bi-2212 single crystal, the B_{1g} and B_{2g} superconducting peaks are clearly distinct in energy and,
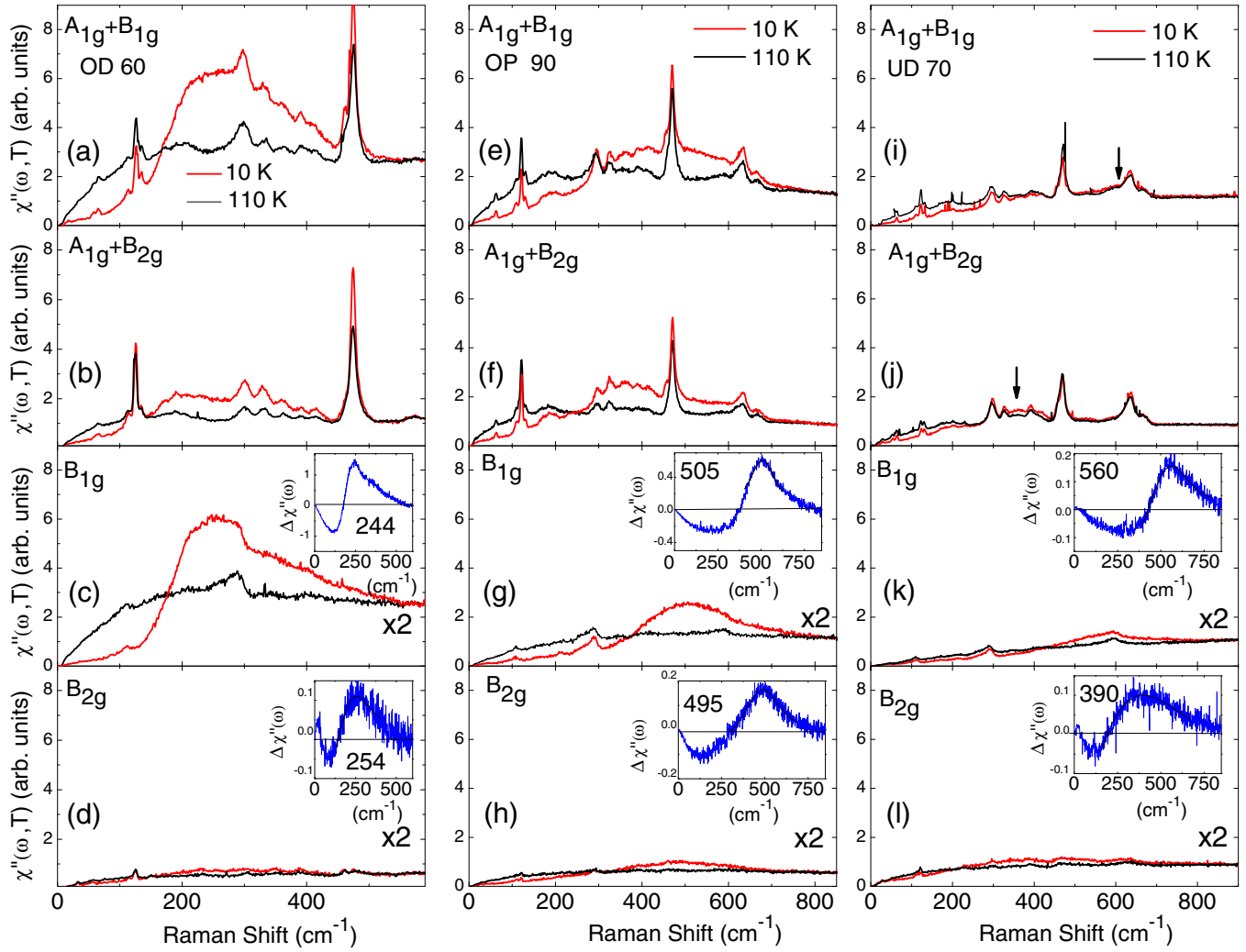
FIG. 1. (Color online) Raman responses $\chi''(\omega, T)$ in $A_{1g}+B_{1g}$, $A_{1g}+B_{2g}$, B_{1g}, and B_{2g} symmetries in the normal and superconducting state of Bi-2212 single crystals for selected doping levels: $p > 0.22$ (OD60), $p = 0.16$ (OP90), and $p = 0.11$ (UD70). The insets show the Raman response at 10 K subtracted from the one at 110 K [$\Delta\chi''(\omega)$]. This allows us to determine the energies of the B_{1g} and B_{2g} electronic peaks.

respectively, located at $560\,\text{cm}^{-1}$ and $390\,\text{cm}^{-1}$ [see insets of Figs. 1(k) and 1(l)]. The weak fingerprints of these two peaks are indicated by black arrows in the $A_{1g}+B_{1g}$ and $A_{1g}+B_{2g}$ spectra [Figs. 1(i) and 1(j)]. On the other hand, the A_{1g} electronic peak is no longer detectable in the UD 70 single crystal.

Importantly, we cannot easily extract the pure A_{1g} electronic spectrum by subtracting the B_{1g} spectrum from the $A_{1g}+B_{1g}$ one (or the B_{2g} spectrum from the $A_{1g}+B_{2g}$ one). There are two reasons for this: (i) the B_{1g} and $A_{1g}+B_{1g}$ spectra (or the B_{2g} and $A_{1g}+B_{2g}$ spectra) were obtained from two distinct crystal orientations (by rotating the crystal), which potentially introduces change in the Raman response intensity; (ii) an additional half-wave plate for measuring the B_{1g} (or B_{2g}) spectrum was used to keep the same polarization at the entrance of the spectrometer as the $A_{1g}+B_{1g}$ (or $A_{1g}+B_{2g}$) spectrum.

In order to circumvent these difficulties and extract the pure A_{1g} electronic contribution, we made two distinct subtractions:

$$\chi''_{A'_{1g}} = \chi''_{A_{1g}+B_{1g}} - \alpha\beta\chi''_{B_{1g}}, \qquad (1)$$

$$\chi''_{A''_{1g}} = \beta\chi''_{A_{1g}+B_{2g}} - \alpha\chi''_{B_{2g}}. \qquad (2)$$

Here, α is the intensity correction factor corresponding to the half-wave plate absorption used in B_{2g} and B_{1g} symmetries, $\alpha = 1.2$, and β is the intensity correction factor linked to the change of the crystal orientation between the B_{1g} and $A_{1g}+B_{1g}$ symmetries (or the B_{2g} and $A_{1g}+B_{2g}$ symmetries).

In order to fix β, we defined two sums [52]:

$$\chi''_{S1} = \chi''_{A_{1g}+B_{1g}} + \alpha\chi''_{B_{2g}}, \qquad (3)$$

$$\chi''_{S2} = \chi''_{A_{1g}+B_{2g}} + \alpha\chi''_{B_{1g}}. \qquad (4)$$

The χ''_{S1} and χ''_{S2} responses were successively obtained after a crystal rotation (see experimental procedure). The β factor is then defined as $\chi''_{S1} = \beta\chi''_{S2}$. The χ''_{S1} (solid line) and $\beta\chi''_{S2}$ (dashed line) responses in the normal and superconducting state are displayed in Figs. 2(c), 2(f), and 2(i). They merge perfectly in the normal and superconducting states, which allows us to estimate β precisely for each doping level. β is close to 1 with a variation of less than 10%.

In Figs. 2(a) and 2(b), 2(d) and 2(e), and 2(g) and 2(h) are displayed the pure A_{1g} Raman spectra extracted in two distinct manners (A'_{1g} and A''_{1g}, respectively) in the normal
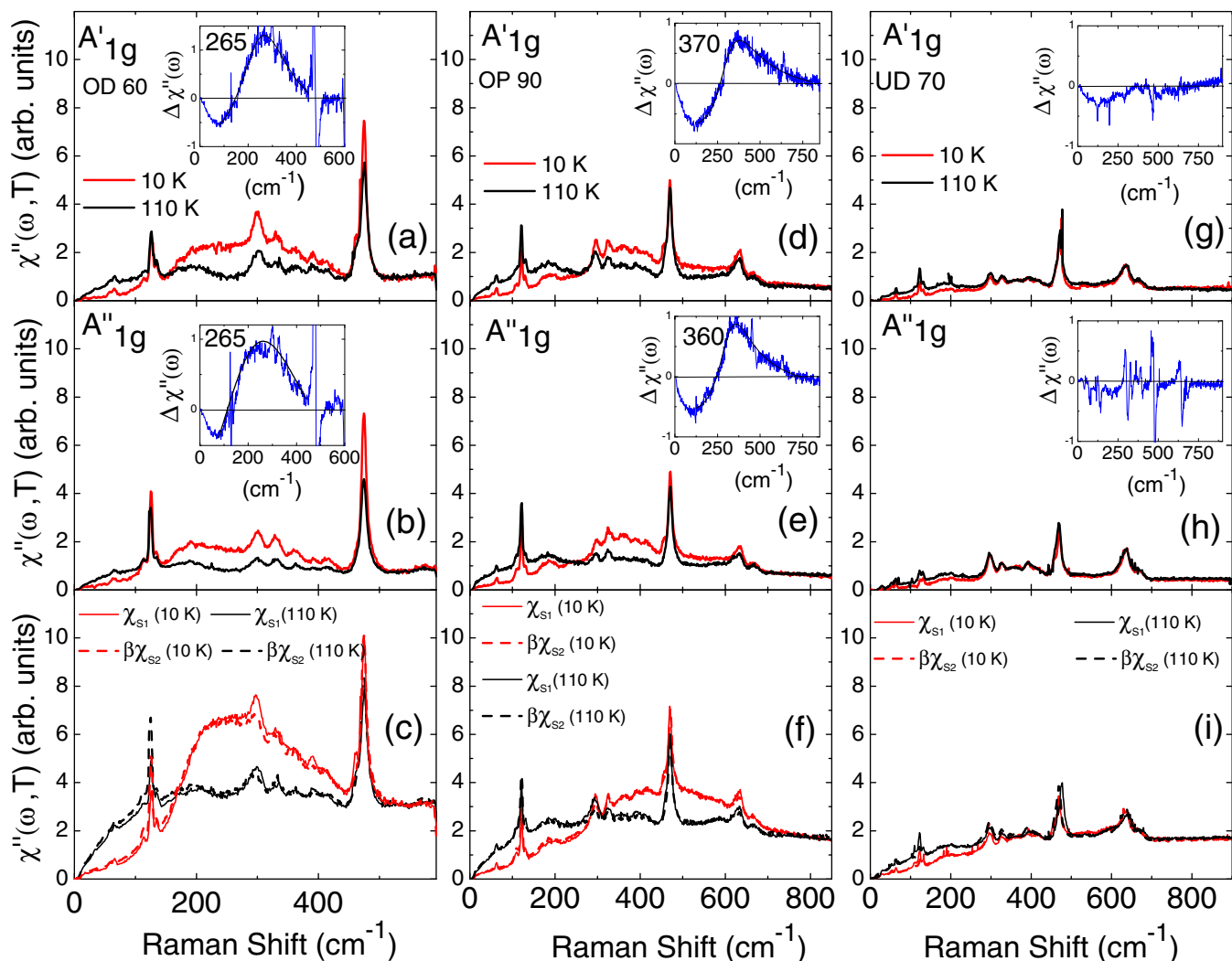
FIG. 2. (Color online) A_{1g} extracted electronic Raman responses in the superconducting state (10 K) and normal state (110 K) for selected doping levels of Bi-2212 single crystals. Here are shown the distinct extractions of the A_{1g} Raman response: A'_{1g} and A''_{1g} associated, respectively, with Eqs. (1) and (2). The insets display the subtracted Raman responses at 10 K from those at 110 K. The Raman responses in (c), (f), and (i) show the sums χ''_{S1} and $\beta\chi''_{S2}$ related to Eqs. (1) and (2). β was defined to make the sums merging.

and superconducting states for the OD60, OP90, and UD70 Bi-2212 single crystals. In the insets, the A_{1g} electronic superconducting peak is revealed by subtracting the normal A_{1g} contribution from the superconducting one. We find well-defined A_{1g} superconducting peaks consistent with each other in both of the cases of extraction, which makes our findings reliable. Interestingly, the energy of the A'_{1g} superconducting peak increases with underdoping (≈ 265 to $\approx 370\,\text{cm}^{-1}$), while the intensity of the A'_{1g} peak decreases before disappearing in the Raman spectra of the UD 70 single crystal [see insets of Figs. 2(a), 2(d), and 2(g)].

In order to get a global view of the doping evolution of the three superconducting peaks detected in the A_{1g}, B_{1g}, and B_{2g} symmetries, the energy of each superconducting peak as a function of doping is plotted in Fig. 3(a).

First, we find that the three energies merge above $p = 0.22$. Below $p = 0.22$, the A_{1g} energy moves away from the B_{1g} and B_{2g} scales. This is confirmed from both extractions (A'_{1g} or A''_{1g}). The A_{1g} scale is no longer detected below $p = 0.12$,

while the B_{1g} and B_{2g} scales are detected until a low-doping level (0.07). The B_{1g} energy scale monotonically increases with underdoping and seems to saturate below $p = 0.12$.

The B_{2g} scale is nonmonotonic and exhibits a maximum close to the optimal doping, $p = 0.16$. Above $p = 0.16$, the B_{2g} decreases and it becomes constant in energy below $p = 0.12$. Our study of the B_{2g} and B_{1g} energy scales at low- and high-doping levels is a refinement of earlier works on Bi-2212 [4,20,46,53–58]. Here we show that the B_{1g} and B_{2g} energy scales vary very slowly below $p = 0.12$ down to $p = 0.06$. The saturation of the B_{1g} superconducting peak in energy was previously reported down to $p \approx 0.11$ and interpreted as a pseudoresonance mode stemming from a strong fermionic self-energy due to the interaction with spin fluctuations [59]. Our extended work to low and high levels of doping reveals two particular ranges: (i) above the $p = 0.22$ (blue/gray) zone in Fig. 3(a) where A_{1g}, B_{1g}, and B_{2g} superconducting peaks merge, and (ii) below the $p = 0.12$ (red/gray) zone in Fig. 3(a) where the B_{1g} and B_{2g} peaks are almost constant in energy.
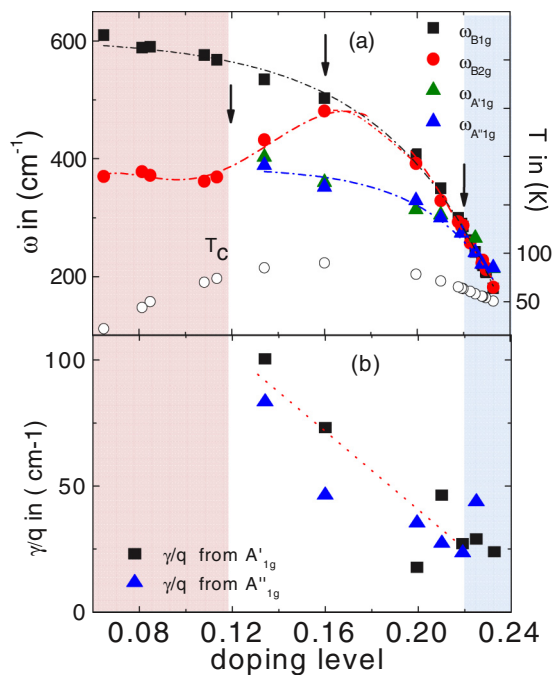
FIG. 3. (Color online) (a) Doping evolutions of the A_{1g}, B_{1g}, and B_{2g} energy scales in the superconducting state. The arrows pinpoint the three special doping levels: Above the $p = 0.22$ (blue/gray) zone, all of the energy scales merge; at $p = 0.16$, the B_{2g} scale is maximum; and below $p = 0.12$, the B_{2g} and B_{1g} scales are almost constant in energy while the A_{1g} one is no longer detectable. Open circles describe the superconducting transition T_c vs p following the Presland-Tallon law [51]. (b) Asymmetric coefficient extracted from A'_{1g} and A''_{1g} superconducting peaks by a standard fit [see Eq. (4)].

This is illustrated in Figs. 4 and 5. In Fig. 4 are displayed the B_{1g}, B_{2g}, and A_{1g} Raman responses of two Bi-2212 single crystals in the superconducting and normal states for $p \geqslant 0.22$. The subtracted Raman responses at 10 K from the one at 110 K show that for OD50 and OD63 compounds, the energies of the B_{1g}, B_{2g}, and A_{1g} peaks coincide with each other see Figs. 4(d)–4(f) and Figs. 4(i)–4(k).

On the other hand, in Fig. 5 are reported selected B_{1g} and B_{2g} Raman responses of underdoped Bi-2212 crystals (below $p = 0.12$) in the superconducting and normal states. The Raman responses measured at 10 K subtracted from the one at 110 K [see insets of Figs. 5(a)–5(f)] show that the B_{1g} energy scale saturates and the B_{2g} scale is almost constant in energy.

Three special doping levels are pinpointed in the evolutions of the A_{1g}, B_{1g}, and B_{2g} scales [see black arrows in Fig. 3(a)]: (i) $p = 0.22$ above which the three energy scales merge, (ii) $p = 0.12$ below which the A_{1g} scale disappears whereas the B_{2g} and B_{1g} scales become constant in energy, and finally (iii) $p = 0.16$ where the B_{2g} scale is peaked and reaches a maximum. We suspect that at least two of these particular doping levels arise from Fermi-surface evolution. It is surprising to find that above $p = 0.22$, the three energy scales merge. We rather expect for a d-wave superconducting gap that the A_{1g}, B_{1g}, and B_{2g} scales have quite distinct energies. Considering a full holelike cylindrical Fermi surface,

the energy ratios between the three scales should be [15] $\omega_{B_{1g}}/\omega_{B_{2g}} \approx 1.3$ and $\omega_{B_{1g}}/\omega_{A_{1g}} \approx 3$, instead of $\omega_{B_{1g}}/\omega_{B_{2g}} \approx \omega_{B_{1g}}/\omega_{A_{1g}} \approx 1$. Such a discrepancy has also been reported in strongly overdoped $Tl_2Ba_2CuO_{6+\delta}$ (Tl-2201) and Y-123 cation-substituted compounds. This has been interpreted as a change of the d-wave gap symmetry into a mixing of a d-wave gap with an s-wave component [60,61]. However, the thermal conductivity measurements in strongly overdoped Tl-2201 showed that nodes are still there [62]. Consequently, we rather believe in a strong alteration of the quasiparticle spectral weight in the antinodal Raman response which modifies the A_{1g}, B_{1g}, and B_{2g} electronic peak positions. This is indeed the case in ARPES measurements on Tl-2201 in the superconducting state, where a quasiparticle anisotropy reversal between the nodes and the antinodes was reported. At high-doping level, the low-energy antinodal Bogoliubov quasiparticle spectral weight is strongly enhanced with respect to the nodal one [63].

In the specific Bi-2212 case, the doping level $p = 0.22$ corresponds to the Lifshitz transition wherein, as a van Hove singularity crosses the chemical potential with underdoping, the electronlike antibonding Fermi surface at high-doping level transforms to be holelike. Such a change in the Fermi-surface topology considerably increases the antinodal quasiparticle spectral weight and can make the three energy scales merge above $p = 0.22$. Preliminary calculations advocate for this scenario, but deeper theoretical investigations are still required and will be developed in the near future. The Lifshitz transition in overdoped Bi-2212 was first observed by ARPES in Bi-2212 [64] and recently detected by the analysis of the integrated Raman intensity as a function of doping level in Bi-2212 [65]. We found that $p = 0.22$ is the starting point of the pseudogap as the doping decreases. The occurrence of a Lifshitz transition at the doping level for which the pseudogap collapses has also been reported in other cuprates [66,67].

On the other hand, when approaching the doping level $p = 0.12$, the Raman intensities of the B_{1g} and A_{1g} peaks are drastically reduced in such a way that the A_{1g} peak is no longer detectable in the Raman spectra [see Figs. 2(g) and 2(h)]. The decrease of the B_{1g} peak intensity [see Figs. 1(c), 1(g), and 1(k)] implies that one of the A_{1g} peaks is also altered because the A_{1g} peak is considered as a bound state of the B_{1g} pairing peak [43,44]. We interpret this significant drop of the peak intensity as a loss of coherent Bogoliubov quasiparticle spectral weight at the antinodes, while the nodal region is protected in the underdoped side of the cuprate phase diagram [16,20,68]. This has been corroborated by (i) ARPES measurements [14,69] and (ii) scanning tunneling spectroscopy (STS), which show that Bogoliubov quasiparticles occupy only a restricted region in the k space around the nodes [70]. We also infer that the Fermi arcs detected in the normal state by ARPES [27] extend into the superconducting state and correspond to a loss of Bogoliubov quasiparticle spectral weight at the antinodes. The antinodal quasiparticles are no longer available for the superconducting state because they are involved in a distinct electronic order. The loss of antinodal quasiparticle spectral weight starts below the pseudogap temperature T^* and it is strongly accentuated by the emergence of the charge ordering as the temperature decreases.
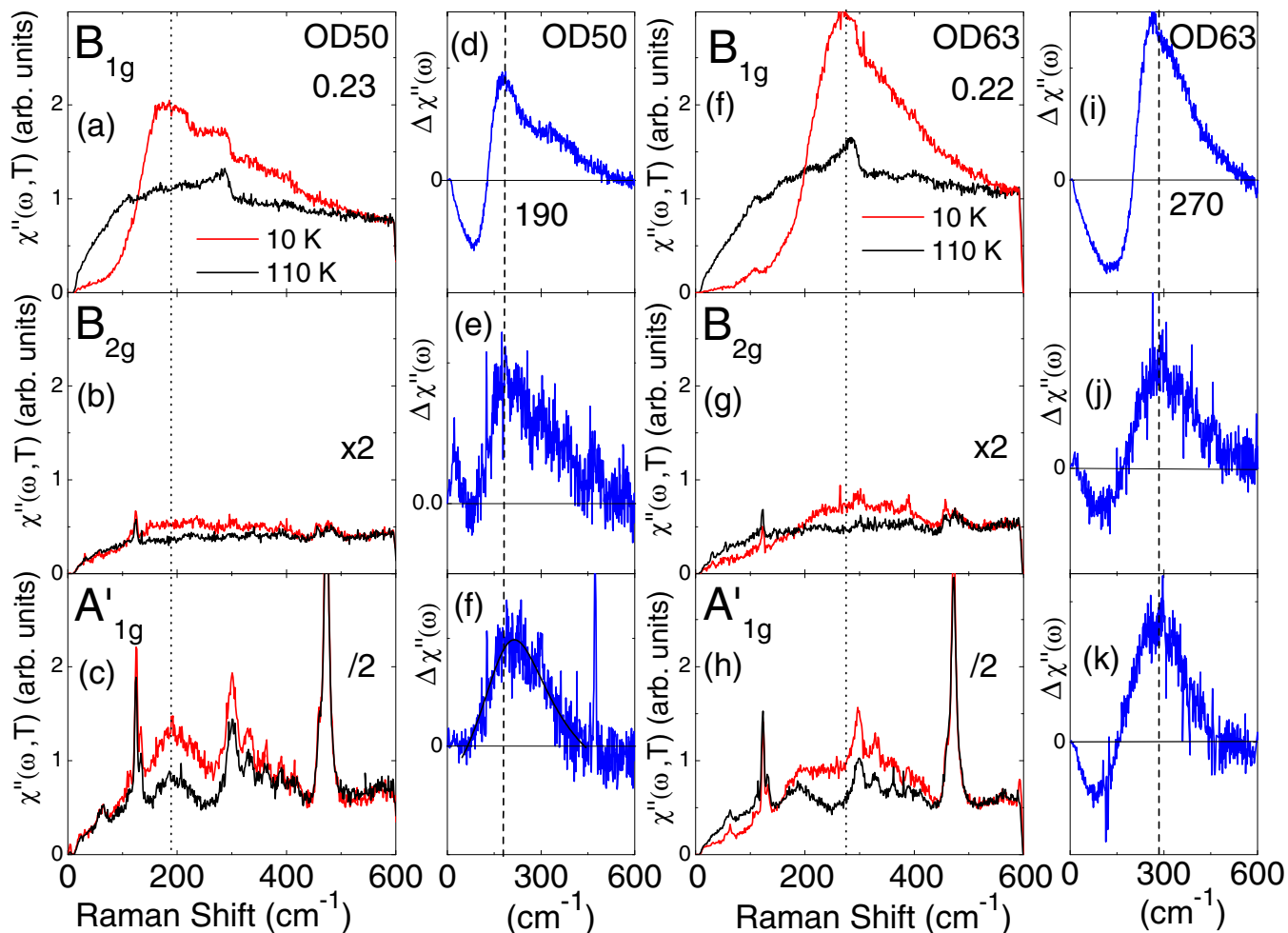
FIG. 4. (Color online) B_{1g}, B_{2g}, and A_{1g} Raman responses in the superconducting (red/gray) and normal (black) states of overdoped Bi-2212 single crystals, (a)–(c) for $p = 0.23$ and (g)–(i) for $p = 0.22$. (d)–(f) and (j)–(l) correspond, respectively, to the subtracted Raman responses at 10 K from the one at 110 K for $p = 0.23$ and $p = 0.22$. The dashed lines show that the locations in energy of the B_{1g}, B_{2g}, and A_{1g} merge for each doping level above $p = 0.22$.

Charge ordering was first proposed from STS measurements in underdoped Bi-2212 [71–73] and then revealed by nuclear magnetic resonance [74,75], resonant x-ray scattering [76–78], and recently confirmed by tunneling [79]. Interestingly, the temperature onset of the Fermi-surface reconstruction defined as the temperature at which the Hall coefficient moves towards negative values in Y-123 [80–82] is also peaked at $p = 0.12$. The observation of a sign change in the Hall coefficient at low temperatures hints that the Fermi surface undergoes a reconstruction into pockets induced by some form of (short-range) charge ordering under high magnetic field [83].

The loss of antinodal spectral weight in the electronic Raman spectra has a clear impact on the B_{1g} and B_{2g} peak energies, as shown in previous works [16–18,20,21,68]. When quasiparticle spectral weight is mostly concentrated around the nodal regions, this pushes back the B_{2g} peak to lower energy and makes larger the B_{1g}/B_{2g} energy ratio with respect to this expected value close to 1.3. This can be seen in Fig. 3(a). At $p = 0.12$, the B_{1g}/B_{2g} ratio is ≈ 1.6 higher than the one expected. The saturation of the pairing gap energy at the antinodes (B_{1g} scale) can then be interpreted as a

competition between superconductivity and charge ordering which prevents an increase of T_c, in agreement with recent investigations [82,84].

Finally, $p = 0.16$ corresponds to the doping level for which the superconducting transition T_c is maximum. This could be the best compromise to enhance superconductivity in a complex medium where several electronic phases compete.

Interestingly, the line shape of the A_{1g} superconducting peak becomes more asymmetric with underdoping [see, for instance, its change in the inset of Fig. 2(d) (OP90) in comparison with the line shape of Fig. 2(a) (OD60)]. We can estimate the line-shape asymmetry as a function of doping by fitting the subtracted Raman responses $\Delta\chi''_{A'_{1g},A'_{1g}}(\omega) = \chi''_{A'_{1g},A'_{1g}}(\omega, 10\,\text{K}) - \chi''_{A'_{1g},A'_{1g}}(\omega, 110\,\text{K})$ by a standard line-shape equation:

$$\Delta\chi''_{A'_{1g},A'_{1g}}(\omega) = \frac{A}{q^2\gamma}\frac{[(\omega - \omega_0)/\gamma + q]^2}{1 + [(\omega - \omega_0)/\gamma]^2}, \tag{5}$$

where A is a renormalization factor and q is the asymmetric coefficient. q tends to infinity for a Lorentzian shape and to a finite value otherwise. γ is the full width at half maximum and
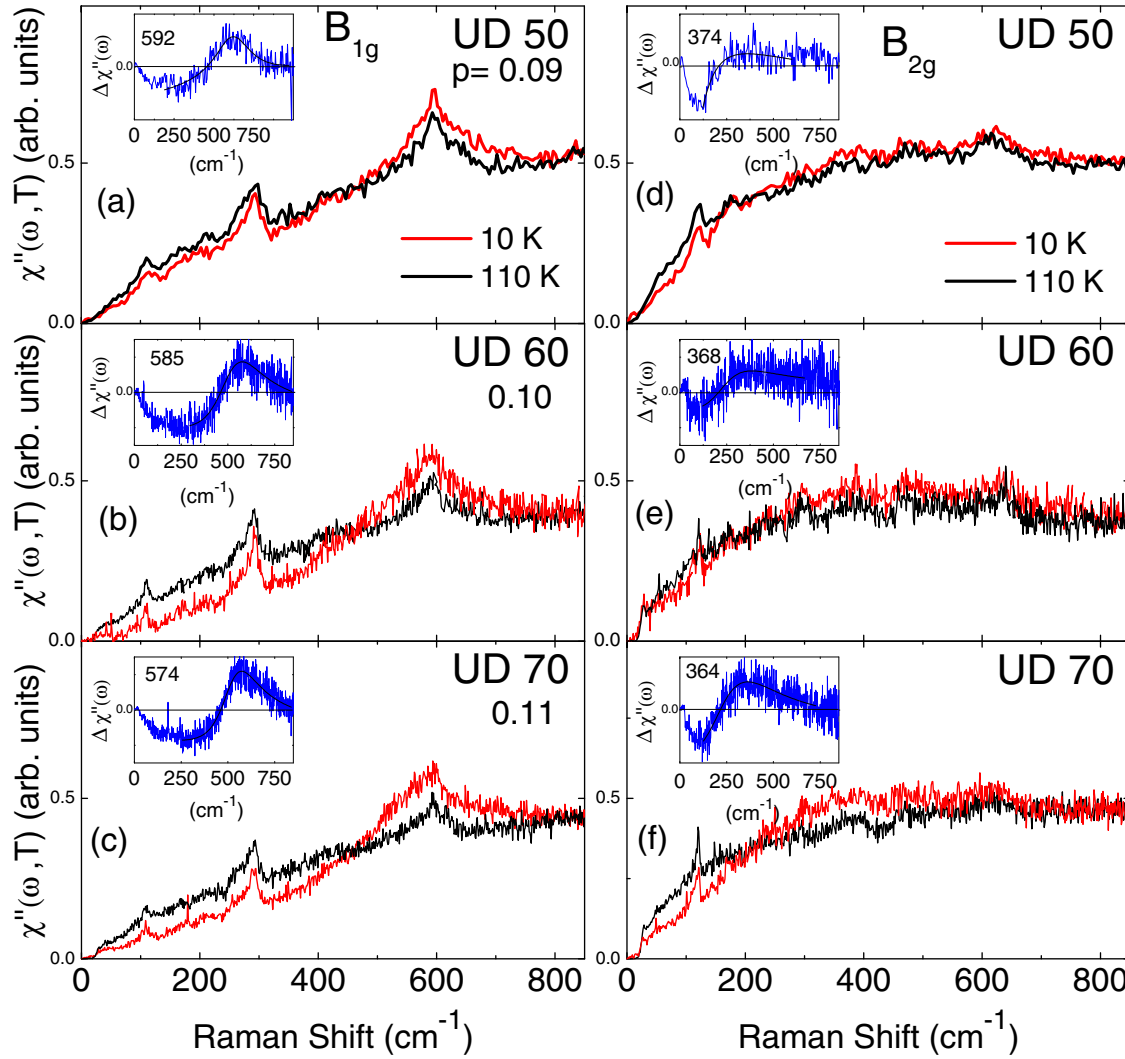
FIG. 5. (Color online) B_{1g} and B_{2g} Raman responses [$\chi''(\omega,T)$] in the superconducting (red/gray) and normal (black) states of selected underdoped Bi-2212 single crystals below $p = 0.12$. The inset in each panel corresponds to the subtracted Raman response [$\Delta\chi''(\omega)$] obtained from measurements at 10 and 110 K. We can notice that both the B_{1g} and B_{2g} electronic peaks are almost constant in energy below $p = 0.12$. Note that the Raman spectra of the UD50 compound was obtained with a 600 g/mm diffraction grating instead of 1800 g/mm one in order to improve the signal/noise ratio and detect the B_{1g} and B_{2g} superconducting peaks, which become weaker in intensity with underdoping. As a consequence, the energy resolution of the UD50 compound is lower than the other doping.

ω_0 is defined such as the A_{1g} peak to take a maximum value at $\omega_m = \omega_0 + \frac{\gamma}{q}$. We chose to report the $\frac{\gamma}{q}$ ratio as the strength of the asymmetric line shape.

The $\frac{\gamma}{q}$ ratio versus doping is plotted in Fig. 3(b). It has been calculated from both $\Delta\chi''_{A'_{1g}}(\omega)$ and $\Delta\chi''_{A''_{1g}}(\omega)$ subtracted responses. We find in both cases an increasing of the asymmetric line shape with underdoping. We suspect this asymmetry comes from the additional contribution 2Δ pairing peak to the A_{1g} peak, as already reported in our previous study [36]. The asymmetric line shape is then enhanced by the increase of the distance in energy between the A_{1g} peak and the 2Δ pairing peak as the doping level is reduced [see Fig. 3(a)].

In conclusion, we have succeeded to extract, in a reliable manner, from electronic Raman scattering, the A_{1g}, B_{1g}, and B_{2g} Raman responses. We find three electronic peaks distinct in energy related to the three symmetries in the superconducting state of Bi-2212. We report a finely tuned doping evolution of

these three electronic peaks by oxygen insertion only into the Bi-2212 structure without cationic substitution. The B_{1g} and A_{1g} increase monotonically as the doping level is reduced, whereas the B_{2g} exhibits a nonmonotonic behavior with a maximum near the optimal doping level. We identify three special doping levels. Above $p = 0.22$, all of the peaks merge in energy [see blue zone in Fig. 3(a)]. Below $p = 0.12$, the A_{1g} is no longer detected, whereas the B_{1g} and B_{2g} scales exhibit two "plateaus" at distinct energies [see red zone in Fig. 3(a)]. Between $p = 0.22$ and $p = 0.12$, the A_{1g} peak and B_{1g} scales increase monotonically, while the B_{2g} scale is nonmonotonic and exhibits a maximum in energy at $p = 0.16$. We suspect that at least the $p = 0.22$ and 0.12 doping levels are directly connected to the doping evolution of the antinodal Bogoliubov quasiparticle spectral weight at low energy. $p = 0.22$ corresponds to the doping level for which a Lifshitz transition occurs [64,65] and the antinodal

quasiparticle spectral weight is strongly increased. On the other hand, $p = 0.12$ corresponds to the doping level for which the charge ordering is well settled [71–77] and the antinodal quasiparticle spectral weight is strongly reduced. Finally, $p = 0.16$ corresponds to the maximum of T_c, where probably the Fermi surface is still disturbed. The B_{1g}, B_{2g}, and A_{1g} peaks all disappear above T_c. The B_{1g} and B_{2g} peaks are two pieces of the 2Δ pairing gap depending on the part of the Fermi surface probed, and the A_{1g} peak is a collective mode related to the 2Δ pairing gap, probably a bound state located below the 2Δ threshold of the particle-hole continuum [44]. Remarkably,

these three superconducting energy scales, although partially detected in other cuprates such as $HgBa_2CuO_{6+\delta}$, (Hg-1201), Y-123, and Tl-1201, are a universal feature to all of the cuprates and reveal competing orders inside the superconducting dome.

[1] J. Bardeen, L. N. Cooper, and J. R. Schrieffer, Phys. Rev. **108**, 1175 (1957).

[2] J. Tallon, G. Williams, M. Staines, and C. Bernhard, Physica C **235–240, Part 3**, 1821 (1994).

[3] G. Deutscher, Nature (London) **397**, 410 (1999).

[4] M. Opel, R. Nemetschek, C. Hoffmann, R. Philipp, P. F. Muller, R. Hackl, I. Tutto, A. Erb, B. Revaz, E. Walker, H. Berger, and L. Forro, Phys. Rev. B **61**, 9752 (2000).

[5] H.-H. Wen, L. Shan, X.-G. Wen, Y. Wang, H. Gao, Z.-Y. Liu, F. Zhou, J. Xiong, and W. Ti, Phys. Rev. B **72**, 134507 (2005).

[6] M. Le Tacon, A. Sacuto, A. Georges, G. Kotliar, Y. Gallais, D. Colson, and A. Forget, Nat. Phys. **2**, 537 (2006).

[7] K. Tanaka, W. S. Lee, D. H. Lu, A. Fujimori, T. Fujii, Risdiana, I. Terasaki, D. J. Scalapino, T. P. Devereaux, Z. Hussain, and Z.-X. Shen, Science **314**, 1910 (2006).

[8] T. Valla, A. V. Fedorov, J. Lee, J. C. Davis, and G. D. Gu, Science **314**, 1914 (2006).

[9] M. C. Boyer, W. D. Wise, K. Chatterjee, M. Yi, T. Kondo, T. Takeuchi, H. Ikuta, and E. W. Hudson, Nat. Phys. **3**, 802 (2007).

[10] J. Tallon and J. Loram, Physica C **349**, 53 (2001).

[11] A. J. Millis, Science **314**, 1888 (2006).

[12] S. Hüfner, M. A. Hossain, A. Damascelli, and G. A. Sawatzky, Rep. Prog. Phys. **71**, 062501 (2008).

[13] W. Guyard, A. Sacuto, M. Cazayous, Y. Gallais, M. Le Tacon, D. Colson, and A. Forget, Phys. Rev. Lett. **101**, 097003 (2008).

[14] T. Kondo, R. Khasanov, T. Takeuchi, J. Schmalian, and A. Kaminski, Nature (London) **457**, 296 (2009).

[15] T. P. Devereaux and R. Hackl, Rev. Mod. Phys. **79**, 175 (2007).

[16] A. Sacuto, Y. Gallais, M. Cazayous, M.-A. Méasson, G. D. Gu, and D. Colson, Rep. Prog. Phys. **76**, 022502 (2013).

[17] X. K. Chen, J. G. Naeini, K. C. Hewitt, J. C. Irwin, R. Liang, and W. N. Hardy, Phys. Rev. B **56**, R513 (1997).

[18] A. V. Chubukov and M. R. Norman, Phys. Rev. B **77**, 214529 (2008).

[19] B. Valenzuela and E. Bascones, Phys. Rev. B **78**, 174522 (2008).

[20] S. Blanc, Y. Gallais, M. Cazayous, M. A. Méasson, A. Sacuto, A. Georges, J. S. Wen, Z. J. Xu, G. D. Gu, and D. Colson, Phys. Rev. B **82**, 144516 (2010).

[21] J. P. F. LeBlanc, J. P. Carbotte, and E. J. Nicol, Phys. Rev. B **81**, 064504 (2010).

[22] I. M. Vishik, M. Hashimoto, R.-H. He, W.-S. Lee, F. Schmitt, D. Lu, R. G. Moore, C. Zhang, W. Meevasana, T. Sasagawa, S. Uchida, K. Fujita, S. Ishida, M. Ishikado, Y. Yoshida, H. Eisaki, Z. Hussain, T. P. Devereaux, and Z.-X. Shen, Proc. Natl. Acad. Sci. USA **109**, 18332 (2012).

[23] H. Alloul, T. Ohno, and P. Mendels, Phys. Rev. Lett. **63**, 1700 (1989).

[24] W. W. Warren, R. E. Walstedt, G. F. Brennert, R. J. Cava, R. Tycko, R. F. Bell, and G. Dabbagh, Phys. Rev. Lett. **62**, 1193 (1989).

[25] A. Abanov, A. V. Chubukov, and J. Schmalian, Adv. Phys. **52**, 119 (2003).

[26] M. R. Norman and J. Lin, Phys. Rev. B **82**, 060509 (2010).

[27] M. R. Norman, H. Ding, M. Randeria, J. C. Campuzano, T. Yokoya, T. Takeuchi, T. Takahashi, T. Mochiku, K. Kadowaki, P. Guptasarma, and D. G. Hinks, Nature (London) **392**, 157 (1998).

[28] N. Doiron-Leyraud, C. Proust, D. LeBoeuf, J. Levallois, J.-B. Bonnemaison, R. Liang, D. A. Bonn, W. N. Hardy, and L. Taillefer, Nature (London) **447**, 565 (2007).

[29] S. E. Sebastian, N. Harrison, and G. G. Lonzarich, Rep. Prog. Phys. **75**, 102501 (2012).

[30] S. E. Sebastian, N. Harrison, F. F. Balakirev, M. M. Altarawneh, P. A. Goddard, R. Liang, D. A. Bonn, W. N. Hardy, and G. G. Lonzarich, Nature (London) **511**, 61 (2014).

[31] N. Doiron-Leyraud, S. Badoux, S. Ren de Cotret, S. Lepault, D. LeBoeuf, F. Laliberté, E. Hassinger, B. J. Ramshaw, D. A. Bonn, W. N. Hardy, R. Liang, J.-H. Park, D. Vignolles, B. Vignolle, L. Taillefer, and C. Proust, Nat. Commun. **6**, 6034 (2015).

[32] S. L. Cooper, F. Slakey, M. V. Klein, J. P. Rice, E. D. Bukowski, and D. M. Ginsberg, Phys. Rev. B **38**, 11934 (1988).

[33] T. Staufer, R. Nemetschek, R. Hackl, P. Müller, and H. Veith, Phys. Rev. Lett. **68**, 1069 (1992).

[34] A. Sacuto, R. Combescot, N. Bontemps, P. Monod, V. Viallet, and D. Colson, Europhys. Lett. **39**, 207 (1997).

[35] Y. Gallais, A. Sacuto, and D. Colson, Physica C **408–410**, 785 (2004).

[36] M. Le Tacon, A. Sacuto, and D. Colson, Phys. Rev. B **71**, 100504 (2005).

[37] J. Rossat-Mignod, L. Regnault, C. Vettier, P. Bourges, P. Burlet, J. Bossy, J. Henry, and G. Lapertot, Physica C **185–189**, Part 1, 86 (1991).

[38] P. Bourges, B. Keimer, S. Pailhès, L. Regnault, Y. Sidis, and C. Ulrich, Physica C **424**, 45 (2005).

[39] V. Hinkov, S. Pailhes, P. Bourges, Y. Sidis, A. Ivanov, A. Kulakov, C. T. Lin, D. P. Chen, C. Bernhard, and B. Keimer, Nature (London) **430**, 650 (2004).

[40] Y. Gallais, A. Sacuto, P. Bourges, Y. Sidis, A. Forget, and D. Colson, Phys. Rev. Lett. **88**, 177401 (2002).

[41] M. Le Tacon, Y. Gallais, A. Sacuto, and D. Colson, J. Phys. Chem. Solids **67**, 503 (2006).

[42] T. Strohm and M. Cardona, Phys. Rev. B **55**, 12725 (1997).

[43] F. Venturini, U. Michelucci, T. P. Devereaux, and A. P. Kampf, Phys. Rev. B **62**, 15204 (2000).

[44] X. Montiel, T. Kloss, C. Pépin, S. Benhabib, Y. Gallais, and A. Sacuto, arXiv:1504.03951.

[45] This is the simple structure commonly used. The distortion between the *a* and *b* crystallographic axes and the incommensurable superstructure modulation have been considered as weak perturbations.

[46] N. Munnikes, B. Muschler, F. Venturini, L. Tassini, W. Prestel, S. Ono, Y. Ando, D. C. Peets, W. N. Hardy, R. Liang, D. A. Bonn, A. Damascelli, H. Eisaki, M. Greven, A. Erb, and R. Hackl, Phys. Rev. B **84**, 144523 (2011).

[47] A. Sacuto, Y. Gallais, M. Cazayous, S. Blanc, M.-A. Méasson, J. Wen, Z. Xu, G. Gu, and D. Colson, C. R. Phys. **12**, 480 (2011).

[48] F. Venturini, Ph.D. thesis, University of Munich, 2003.

[49] J. Wen, Z. Xu, G. Xu, M. Hcker, J. Tranquada, and G. Gu, J. Cryst. Growth **310**, 1401 (2008).

[50] L. Mihaly, C. Kendziora, J. Hartge, D. Mandrus, and L. Forro, Rev. Sci. Instrum. **64**, 2397 (1993).

[51] M. Presland, J. Tallon, R. Buckley, R. Liu, and N. Flower, Physica C **176**, 95 (1991).

[52] M. L. Tacon, Ph.D. thesis, Université Paris Diderot, Paris 7, 2006.

[53] G. Blumberg, M. Kang, M. V. Klein, K. Kadowaki, and C. Kendziora, Science **278**, 1427 (1997).

[54] L. V. Gasparov, P. Lemmens, N. N. Kolesnikov, and G. Güntherodt, Phys. Rev. B **58**, 11753 (1998).

[55] J. G. Naeini, X. K. Chen, J. C. Irwin, M. Okuya, T. Kimura, and K. Kishio, Phys. Rev. B **59**, 9642 (1999).

[56] S. Sugai and T. Hosokawa, Phys. Rev. Lett. **85**, 1112 (2000).

[57] K. C. Hewitt and J. C. Irwin, Phys. Rev. B **66**, 054516 (2002).

[58] T. Masui, M. Limonov, H. Uchiyama, S. Lee, S. Tajima, and A. Yamanaka, Phys. Rev. B **68**, 060506 (2003).

[59] A. V. Chubukov and D. K. B. G. Morr, Solid State Commun. **112**, 183 (1999).

[60] K. Nishikawa, T. Masui, S. Tajima, H. Eisaki, H. Kito, and A. Iyo, J. Phys. Chem. Solids **69**, 3074 (2008).

[61] T. Masui, T. Hiramachi, K. Nagasao, and S. Tajima, Phys. Rev. B **79**, 014511 (2009).

[62] C. Proust, E. Boaknin, R. W. Hill, L. Taillefer, and A. P. Mackenzie, Phys. Rev. Lett. **89**, 147003 (2002).

[63] M. Platé, J. D. F. Mottershead, I. S. Elfimov, D. C. Peets, R. Liang, D. A. Bonn, W. N. Hardy, S. Chiuzbaian, M. Falub, M. Shi, L. Patthey, and A. Damascelli, Phys. Rev. Lett. **95**, 077001 (2005).

[64] A. Kaminski, S. Rosenkranz, H. M. Fretwell, M. R. Norman, M. Randeria, J. C. Campuzano, J.-M. Park, Z. Z. Li, and H. Raffy, Phys. Rev. B **73**, 174511 (2006).

[65] S. Benhabib, A. Sacuto, M. Civelli, I. Paul, M. Cazayous, Y. Gallais, M. A. Méasson, R. D. Zhong, J. Schneeloch, G. D. Gu, D. Colson, and A. Forget, Phys. Rev. Lett. **114**, 147001 (2015).

[66] A. Ino, C. Kim, M. Nakamura, T. Yoshida, T. Mizokawa, A. Fujimori, Z.-X. Shen, T. Kakeshita, H. Eisaki, and S. Uchida, Phys. Rev. B **65**, 094504 (2002).

[67] A. Piriou, N. Jenkins, C. Berthod, I. Maggio-Aprile, and O. Fischer, Nat. Commun. **2**, 221 (2011).

[68] S. Blanc, Y. Gallais, A. Sacuto, M. Cazayous, M. A. Méasson, G. D. Gu, J. S. Wen, and Z. J. Xu, Phys. Rev. B **80**, 140502 (2009).

[69] H. Ding, J. R. Engelbrecht, Z. Wang, J. C. Campuzano, S. C. Wang, H. B. Yang, R. Rogan, T. Takahashi, K. Kadowaki, and D. G. Hinks, Phys. Rev. Lett. **87**, 227001 (2001).

[70] Y. Kohsaka, C. Taylor, P. Wahl, A. Schmidt, J. Lee, K. Fujita, J. W. Alldredge, K. McElroy, J. Lee, H. Eisaki, S. Uchida, D.-H. Lee, and J. C. Davis, Nature (London) **454**, 1072 (2008).

[71] K. McElroy, D.-H. Lee, J. E. Hoffman, K. M. Lang, J. Lee, E. W. Hudson, H. Eisaki, S. Uchida, and J. C. Davis, Phys. Rev. Lett. **94**, 197005 (2005).

[72] W. D. Wise, M. C. Boyer, K. Chatterjee, T. Kondo, T. Takeuchi, H. Ikuta, Y. Wang, and E. W. Hudson, Nat. Phys. **4**, 696 (2008).

[73] C. V. Parker, P. Aynajian, E. H. da Silva Neto, A. Pushp, S. Ono, J. Wen, Z. Xu, G. Gu, and A. Yazdani, Nature (London) **468**, 677 (2010).

[74] T. Wu, H. Mayaffre, S. Krämer, M. Horvatic, C. Berthier, W. N. Hardy, R. Liang, D. A. Bonn, and M.-H. Julien, Nature (London) **477**, 191 (2011).

[75] T. Wu, H. Mayaffre, S. Krämer, M. Horvatić, C. Berthier, W. N. Hardy, R. Liang, D. A. Bonn, and M.-H. Julien, Nat. Commun. **6**, 6438 (2015).

[76] G. Ghiringhelli, M. Le Tacon, M. Minola, S. Blanco-Canosa, C. Mazzoli, N. B. Brookes, G. M. De Luca, A. Frano, D. G. Hawthorn, F. He, T. Loew, M. M. Sala, D. C. Peets, M. Salluzzo, E. Schierle, R. Sutarto, G. A. Sawatzky, E. Weschke, B. Keimer, and L. Braicovich, Science **337**, 821 (2012).

[77] J. Chang, E. Blackburn, A. T. Holmes, N. B. Christensen, J. Larsen, J. Mesot, R. Liang, D. A. Bonn, W. N. Hardy, A. Watenphul, M. v. Zimmermann, E. M. Forgan, and S. M. Hayden, Nat. Phys. **8**, 871 (2012).

[78] E. H. da Silva Neto, P. Aynajian, A. Frano, R. Comin, E. Schierle, E. Weschke, A. Gyenis, J. Wen, J. Schneeloch, Z. Xu, S. Ono, G. Gu, M. Le Tacon, and A. Yazdani, Science **343**, 393 (2014).

[79] K. Fujita, C. K. Kim, I. Lee, J. Lee, M. Hamidian, I. A. Firmo, S. Mukhopadhyay, H. Eisaki, S. Uchida, M. J. Lawler, E. A. Kim, and J. C. Davis, Science **344**, 612 (2014).

[80] D. LeBoeuf, N. Doiron-Leyraud, J. Levallois, R. Daou, J.-B. Bonnemaison, N. E. Hussey, L. Balicas, B. J. Ramshaw, R. Liang, D. A. Bonn, W. N. Hardy, S. Adachi, C. Proust, and L. Taillefer, Nature (London) **450**, 533 (2007).

[81] N. Doiron-Leyraud, S. Lepault, O. Cyr-Choinière, B. Vignolle, G. Grissonnanche, F. Laliberté, J. Chang, N. Barišić, M. K. Chan, L. Ji, X. Zhao, Y. Li, M. Greven, C. Proust, and L. Taillefer, Phys. Rev. X **3**, 021019 (2013).

[82] O. Cyr-Choinière, D. LeBoeuf, S. Badoux, S. Dufour-Beausejour, D. A. Bonn, W. N. Hardy, R. Liang, N. Doiron-Leyraud, and L. Taillefer, arXiv:1503.02033v1.

[83] G. Grissonnanche, F. Laliberté, S. Renéde Cotret, A. Juneau-Fecteau, S. Dufour-Beauséjour, O. Cyr-Choinière, M. È. Delage, D. LeBoeuf, J. Chang, B. J. Ramshaw, D. A. Bonn, W. N. Hardy, R. Liang, S. Adachi, N. E. Hussey, B. Vignolle, C. Proust, M. Sutherland, S. Krämer, J. H. Park, D. Graf, N. Doiron-Leyraud, and L. Taillefer, arXiv:1508.05486.

[84] O. Cyr-Choiniere, G. Grissonnanche, S. Badoux, J. Day, D. A. Bonn, W. N. Hardy, R. Liang, N. Doiron-Leyraud, and L. Taillefer, arXiv:1504.06972.